Bioconvective flow of microorganisms in an Eyring-Powell nanofluid with activation energy over a curved surface

[a]M. Imran and [a]M. Naveed[*]

[a]Department of Mathematics, Division of Science and Technology,
University of Education, Lahore 54770, Pakistan

Abstract: The current theoretical study focuses on the effects of microorganisms and activation energy in bio-convective flow of Eyring-Powell nanofluid on a stretchable curved surface with influences of thermophoretic and Brownian diffusions. The nonlinear flow equations depicting the rheological features of the Eyring-Powell fluid are developed by adopting the curvilinear coordinate scheme. The activation energy has been added to sense its importance on the concentration of nanoparticles, whereas motile microorganisms are included in order to stabilize the nanofluid suspension. The entropy generation analysis is aimed at analyzing the system irreversibility with reference to answer questions about energy dissipation and thermal efficiency. Moreover, the equations of velocity and energy are defined by the effects of a magnetic field and heat generation, respectively. The velocity, temperature, nanoparticle concentration, microorganism concentration, entropy production, and the profiles of the local numbers are represented with numerical solutions derived using the shooting technique. The effects of the influential variables on profiles of concern are examined in detail through graphical and tabular results. The graphical results state that concentration profile of nanoparticles is enhanced with increased values of the activation energy parameter and decreases with temperature difference constant, the reaction rate variable, and the fitted rate constant. This study develops the understanding of movement of nanofluid over curved surfaces and provides a comprehensive background that extends existing literature, offering insights into multi-physics transport processes relevant to advanced manufacturing, chemical processing, bioengineering, and thermal management applications, including polymer extrusion, catalytic reactors, biomedical drug delivery, electronic cooling, and bioreactor design.

Keywords: curved stretchy surface, activation energy, Eyring-Powell nanofluid, entropy production, gyrotactic microorganisms, Numerical solution.

1. Introduction

In recent years, significant attention has been devoted to boundary layer stretchy flows across curved geometries with varying surface velocities due to their broad applications in numerous technological and manufacturing procedures. These include wire drawing, fiber spinning, hot rolling, artificial fiber production, continuous stretching of plastic films, polymer extrusion, glass manufacturing, tower distillation, aerodynamics, electronic chip cooling, extrusion of elastic sheets, and paper production. In such arenas, the attribute of the final product is strongly affected by the surface velocity and stretched rate. Sajid et al. [1] were among the pioneers in investigating viscous liquid motion on a stretching curvy surface and analyzing the role of

[*] Corresponding Author. Tel.: +92 312 6490512

e-mail address: muhammad.naveed@ue.edu.pk (M. Naveed)

curvature radius on the flow field. Shabbir et al. [2] extended this by exploring micropolar liquid flow over a nonlinearly curved stretchy sheet. Ahmad et al. [3] studied heat transfer characteristics in Williamson nanofluid flow past a curvy exponential stretched wall with temperature-dependent conductivity. Imran and Naveed [4] performed a comparative analysis on activation energy and thermophoretic effects in Carreau nanofluid flow via a curvy surface. Similarly, Naveed et al. [5] examined the influence of homogeneous–heterogeneous chemical reactions on viscous liquid flow because of an oscillating curved stretchy surface. Further literature on curved geometries in fluid flow can be found in references [6–10].

Many real-life fluids that deviate from Newton's law of viscosity and exhibit a nonlinear relationship between shear stress and strain rate are categorized as non-Newtonian fluids. Examples include soap solutions, yogurt, shampoo, ketchup, blood, clay suspensions, lubricants, polymer melts, and certain industrial oils. These fluids are widely encountered in chemical and nuclear engineering, polymer processing, petroleum industries, bioengineering, and food technology. To examine their complex behavior a variety of non-Newtonian fluid models have been proposed. Amongst different non-Newtonian fluid models the Eyring–Powell model is a prominent time-independent model depicting the molecular kinetics and rate process theory. This fluid model effectively characterizes both shear- thickening and shear-thinning behaviors and avoids singularities at zero shear rate, unlike traditional power-law models. It has been used to model polymeric fluids, lubricants and biological fluids like blood and synovial fluid Khan et al. [11] examined the flow of magnetized Eyring- Powell fluid using modified Fourier law and Fick law towards a curved surface. Naveed et al. [12] investigated the influence of melting heat transference in a flow of Eyring-Powell fluid via a curvy channel. Different aspects of flow and heat transfer analysis in Eyring-Powell fluid for different flow geometries has been examined by various researchers. For more details the interested readers are referred to the articles [13-15] and reference therein.

Due to its significant ability to increase the rate of thermal conductivity and heat transfer, nanofluids have received important consideration in last few years in various disciples of engineering and industrial applications point of view. These fluids are made up by dispersing nanoscale particles into conventional base fluids, which have prominent thermophysical properties as compared to traditional coolants. As a result, nanofluids have been remarkably examined in thermal management systems, including heat exchangers, radiators and electronic cooling devices. The applications of nanofluids are also found in microprocessors, in advanced technologies such as micro-electromechanical systems (MEMS) and welding equipment. Furthermore, nanofluids play a vital role in automotive thermal systems by effectively cooling internal combustion engines and electric vehicle components. In the biomedical domain, they are being investigated for applications in targeted drug delivery, hyperthermia cancer therapy, and bio-imaging, due to their enhanced thermal response and biocompatibility. Jafaripournimchahi et al. [16] have studied the features of thermal radiation and magnetic field in the mixed convective flow of hybrid nano liquid towards a vertical wall. Abbas et al. [17] have analyzed the stimulus of HH reactions in the movement of a non-Newtonian nano liquid across an oscillating curvy wall. Nandeppanavar et al. [18] have inspected Prandtl-Eyring nanofluid in the presence of a permeable medium towards a stretched sheet. Haq et al. [19]

have performed a numerical investigation to examine the significance of Brownian motion and thermophoretic in the Carreau liquid motion. Very lately, Imran et al. [20] conducted analytical research and calculated the stimulus of thermophoresis and Brownian diffusion in the bioconvective flow of viscous fluid inside a curvy oscillating channel. For a more comprehensive review of nanofluid studies across various geometries, the reader is referred to the literature [21–30].

The processes of heat and mass transfer are essential in many industrial and engineering processes especially when they are accompanied by chemical reactions. Activation energy which is the minimum energy needed to cause a chemical reaction is a critical factor that affects these procedures. Activation energy plays a very important role in the reaction kinetics in the reactive flows, thus changing the velocity of mass diffusion and heat transport. This aspect is particularly noteworthy in such applications as geothermal systems, chemical processing, material oxidation as well as food engineering. The effects of activation energy on the behaviour of non-Newtonian and nanofluid systems is that it determines the thermal stability and the behaviour of the boundary layer by changing the velocity and concentration fields. Haider et al. [31] determined the significance of activation energy on the unsteady flow of nanofluid over a stretching sheet with Stefan blowing impacts. Kumar et al. [32] explored the consequences of activation energy in hybrid nanofluid motion past a curved sheet. Ali et al. [33] considered the effects of activation energy along with a modified form of Fourier's theory in the flow of nanofluid via a rotating surface. Ahmad and Khan [34] examined heat and mass transfer effects on nanofluid motion with activation Arrhenius energy across a permeable curvy surface. Reddy et al. [35] analyzed the dynamics of activation energy in the magnetized nanofluid towards a stretchable sheet. The stimulus of activation energy and heat production in the magnetized flow of Maxwell liquid over a permeable plate was determined by Sudarmozhi et al. [36]. Ahmad et al. [37] performed numerical simulations for non-linear radiative and magnetized flow of a non-Newtonian nano liquid with activation energy.

Bioconvective flow refers to the self-organized convective motion in a fluid encouraged by the collective behavior of motile microorganisms, such as gyrotactic algae or bacteria, which typically swim upward against gravity. This vertical motion produces an irregular density gradient with the microorganisms mostly congregating towards the top resulting in gravitational instability and consequently initiating convection. The resulting bioconvection mixes and transports heat, mass and nutrients in the fluid significantly. The effect is crucial in many biological and industrial fields, such as bioreactors, biofuel, wastewater decontamination, and microfluidic equipment designs. Hayat et al. [38] examined the stimulus of bioconvection, which consists of gyrotactic microorganisms on Prandtl-Eyring flow, across a stretchy sheet. Significance of bioconvection in EMHD hybrid nanofluid via a permeable sheet was determined by Rashed et al. [39]. Sarma and Sarma [40] organized a numerical study to assess the influence of microorganisms in bioconvective time-dependent flow of Casson fluid past a vertical plate. Analysis of bioconvective flow of non-Newtonian liquid over a permeable curved stretched surface was done by Ahsan et al. [41]. Hamid et al. [42] conducted a computational study on the bioconvective flow of nanofluid towards a bidirectional sheet containing microorganisms in a permeable medium. Further comprehensive details on the

bioconvective flow of fluids with divergent rheological models across diverse geometries are referred to reference [43-45] and the references cited therein.

Entropy production plays a crucial role in assessing the thermodynamic irreversibility of transport processes occurring within fluid flow systems. It serves as a vital indicator of energy degradation, particularly in thermal systems where heat and mass transfer, and chemical reactions are present. The study of entropy production can be used to optimize the performance of a system in which the flow of a fluid across the edges of a stretching surface is of interest (polymer processing, thermal coating, and biofluid transport) to determine where the thermodynamic inefficiencies in a system exist. High entropy generation is generally linked to a high degree of irreversibility which may reduce the overall efficiency of the heat and mass transfer processes. Hence, the reduction of the entropy creation is the key to the improvement of the performance and sustainability of thermal systems. The use of complex working fluids, including nanofluids and hybrid nanofluids implies additional need of entropy analysis, as these fluids are characterized by complex microscale interactions and therefore can have an important impact on the thermodynamic behavior of the system. Sadighi et al. [46], Swamy et al. [47], and Imran et al. [48] examined the entropy generation in different conditions of magnetized and vibrating flows. Mandal et al. [49] and Yazdi et al. [50] also provided the understanding of the entropy production in nanoparticles laden fluids under varying thermal and geometrical conditions.

The current paper proposes a new and complete model to estimate bioconvective flow of an Eyring-Powell nanofluid over a curved stretching surface, the combination of the activation energy, thermophoretic, and Brownian diffusion, and the analysis of the entropy production. This work is the first to bring together non-Newtonian rheology with curvilinear stretching geometry, dynamics of nanoparticles and bioconvection by microorganisms in a single model unlike the earlier studies, which mainly focused on either flat geometry or Newtonian base liquids or isolated physical systems. Realistic representation of complex industrial fluids is included with the addition of the Eyring-Powell model that describes the effects of shear-thinning and shear-thickening without singularities. Also, the interaction of the action of energy with the effects of bioconvective in a curved geometry is not widely studied. The analysis of thermodynamic irreversibility is also quantified by the study through a careful analysis of entropy production, which is useful in optimization of thermal systems that consume less energy. This integrated approach significantly extends existing literature and provides a deeper understanding of multi-physics transport processes relevant to advanced manufacturing, chemical processing, and bioengineering applications, such as polymer extrusion, catalytic reactors, biomedical drug delivery, electronic cooling, and bioreactor design.

2. Development of the problem

Consider an electrically conducting, incompressible, bioconvective, and steady motion of Eyring-Powell nano liquid in the presence of gyrotactic microorganisms towards a stretchable curved surface looped in a semi-circle form with radius R_α (see Fig. 1). A uniform magnetic field of power M_0 is executed along the radial $r-$direction. The influences of the induced

magnetic field are ignored because of the consideration of the very low magnetic Reynolds number. Let C_w, T_w, and N_w signifies surface temperature, nanoparticle concentration at the surface, and the concentration of the microorganisms at the sheet. Similarly, let C_∞, N_∞, and T_∞ represent the ambient concentrations of the nanoparticles and microorganisms and ambient temperature, respectively, with $C_\infty < C_w$, $N_w > N_\infty$, and $T_\infty < T_w$. Under these presumptions, the governing equations for energy, velocity, continuity, nanoparticles, and microorganisms' concentration are given as [4, 9, 11, 12, 15]

$$\frac{\partial w}{\partial r}+\frac{w}{\left(R_\alpha+r\right)}+\frac{\partial v}{\partial c}\frac{R_\alpha}{\left(R_\alpha+r\right)}=0, \tag{1}$$

$$\frac{\partial p}{\partial r}=\frac{\rho v^2}{\left(r+R_\alpha\right)}, \tag{2}$$

$$\begin{aligned} &w\frac{\partial v}{\partial r}+\frac{wv}{\left(R_\alpha+r\right)}+\frac{R_\alpha v}{\left(R_\alpha+r\right)}\frac{\partial v}{\partial c}=-\frac{1}{\rho_f}\frac{R_\alpha}{\left(R_\alpha+r\right)}\frac{\partial p}{\partial c}+\left(\nu_1+\frac{1}{\rho_f Ba}\right)\left(\frac{\partial^2 v}{\partial r^2}+\frac{\partial v}{\partial r}\frac{1}{\left(R_\alpha+r\right)}-\frac{v}{\left(R_\alpha+r\right)^2}\right)\\ &-\frac{1}{6\rho_f Ba}\left(\begin{array}{l}3\frac{\partial^2 v}{\partial r^2}\left(\frac{\partial v}{\partial r}\right)^2-\left(\frac{\partial v}{\partial r}\right)^3\frac{1}{\left(R_\alpha+r\right)}+\frac{3v}{\left(R_\alpha+r\right)^2}\left(\frac{\partial v}{\partial r}\right)^2+\frac{3v^2}{\left(R_\alpha+r\right)^2}\frac{\partial^2 v}{\partial r^2}+\frac{v^3}{\left(R_\alpha+r\right)^4}\\ -\frac{6v}{\left(R_\alpha+r\right)}\frac{\partial v}{\partial r}\frac{\partial^2 v}{\partial r^2}-\frac{3v^2}{\left(R_\alpha+r\right)^3}\frac{\partial v}{\partial r}\end{array}\right)-\frac{\sigma}{\rho_f}M_0^2 v\\ &+\frac{1}{\rho_f}\left(\left(1-C_\infty\right)\rho_f B_1^* g^*\left(T-T_\infty\right)-\left(\rho_p-\rho_f\right)g^*\left(C^*-C_\infty\right)-\left(N^*-N_\infty\right)g^*\gamma^*\left(\rho_n-\rho_f\right)\right), \end{aligned} \tag{3}$$

$$w\frac{\partial T}{\partial r}+\frac{R_\alpha v}{\left(r+R_\alpha\right)}\frac{\partial T}{\partial c}-\frac{Q_0\left(T-T_\infty\right)}{\left(c_1\rho\right)_f}=\kappa\left(\frac{\partial^2 T}{\partial r^2}+\frac{1}{\left(r+R_\alpha\right)}\frac{\partial T}{\partial r}\right)+\tau_\alpha\left(\frac{D_T}{T_w}\left(\frac{\partial T}{\partial r}\right)^2+D_\beta\left(\frac{\partial C^*}{\partial r}\frac{\partial T}{\partial r}\right)\right), \tag{4}$$

$$\begin{aligned} &w\frac{\partial C^*}{\partial r}+\frac{\partial C^*}{\partial c}\frac{vR_\alpha}{\left(r+R_\alpha\right)}=D_\beta\left(\frac{\partial^2 C^*}{\partial r^2}+\frac{\partial C^*}{\partial r}\frac{1}{\left(r+R_\alpha\right)}\right)+\frac{D_T}{T_\infty}\left(\frac{\partial^2 T}{\partial r^2}+\frac{1}{\left(r+R_\alpha\right)}\frac{\partial T}{\partial r}\right)\\ &-k_r^2\left(\frac{T}{T_\infty}\right)^m\left(C^*-C_\infty\right)\mathrm{Exp}\left(\frac{-E_a}{\chi T}\right), \end{aligned} \tag{5}$$

$$w\frac{\partial N^*}{\partial r}+\frac{\partial N^*}{\partial c}\frac{vR_\alpha}{\left(r+R_\alpha\right)}=D_n\left(\frac{\partial^2 N^*}{\partial r^2}+\frac{\partial N^*}{\partial r}\frac{1}{\left(r+R_\alpha\right)}\right)-\frac{b_a W_a}{C_w-C_\infty}\frac{\partial}{\partial r}\left(N^*\frac{\partial C^*}{\partial r}\right), \tag{6}$$

With bcs [9, 11, 15]

$$\left.\begin{aligned} &v=b_1 c,\ \ C^*=C_w,\ T=T_w,\ N^*=N_w,\ \ w=0\ \text{ at } r=0,\\ &C^*\to C_\infty,\ N^*\to N_\infty,\ T^*\to T_\infty,\ \frac{\partial v}{\partial r}\to 0,\ v\to 0\ \text{ as } r\to\infty. \end{aligned}\right\} \tag{7}$$

Here (v, w) characterizes the parts of the liquid velocity in (c, r) directions, $\tau_\alpha = (\rho_p c_{1p}) / (c_{1f} \rho_f)$ correspond to the ratio of the nanoparticles' thermal capacity to the thermal capacitance of the base fluid, ρ_f is the base liquid density, p is the pressure, b_1 defines the stretchable rate of the surface, χ is the Boltzmann constant, D_β and D_T are the Brownian diffusion and thermophoretic variables, ν_1 embodies the kinematic viscosity, m is the fitted rate constant, κ is the thermal diffusivity, T, N^*, and C^* represents the temperature of the liquid, microorganism, and nanoparticle concentration, σ is the electrical conductivity, ρ_p and ρ_n are the densities of nanoparticles and microorganisms, B and a are the Eyring-Powell liquid parameters, Q_0 is the heat production variable, D_n is the microorganism's diffusion coefficient, k_r^2 is the chemical reaction rate constant, b_a is the chemotaxis constant, W_a is the speed of cells, E_a is the activation energy parameter, g^*, β_1^*, and γ^* are the gravity, the volume expansion coefficient, and the average volume of microorganisms, respectively.

A similar solution is achieved by involving the following variables [4, 9, 11, 15]

$$v = b_1 c\, g'(\zeta),\ \zeta = r\sqrt{\frac{b_1}{\nu_1}} =,\ N_\infty + (N_w - N_\infty)\Psi(\zeta) = N^*,\ w = \frac{-R_\alpha}{R_\alpha + r}\sqrt{b_1 \nu_1}\, g(\zeta),$$
$$\Phi(\zeta) = C^* - C_\infty / (C_w - C_\infty),\ p = \rho b_1^2 c^2 P(\zeta),\ T_\infty = T - (T_w - T_\infty)\Theta(\zeta). \tag{8}$$

In the above equation g', and g are the dimensionless horizontal and vertical components of the velocity and temperature of the fluid, Φ is the dimensionless concentration of the nanoparticles, Θ is the temperature of the fluid, Ψ is the dimensionless concentration of microorganisms, P is the dimensionless pressure of the fluid, and ζ is the dimensionless similarity variable. By incorporating Eq. (8), Eq. (1) is verified identically, and the rest of the Eqs. (2, 3, 4, 5, 6) and (7) reduce as

$$\frac{\partial P(\zeta)}{\partial \zeta} = \frac{g'^2}{\eta + R_c}, \tag{9}$$

$$2R_c P(\eta) = (1+\alpha)\left((\zeta + R_c)g''' - \frac{g'}{(\zeta + R_c)} + g''\right) + \gamma(\zeta + R_c)\Theta - \gamma(\zeta + R_c)N_r\Phi - \gamma(\zeta + R_c)R_b\Psi$$
$$-\alpha\beta\left(\begin{array}{l} 3(\zeta + R_c)g''^2 g''' + \frac{3g'g''^2}{(\zeta + R_c)} + \frac{3}{(\zeta + R_c)}g'''g'^2 \\ -\frac{3g'^2 g''}{(\zeta + R_c)^2} + \frac{g'^3}{(\zeta + R_c)^3} - 6g'''g'g'' - g''^3 \end{array}\right) - g'M^2(\zeta + R_c) + R_c(g\,g'' - g'^2) + \frac{R_c\, g'\, g}{(\zeta + R_c)}, \tag{10}$$

$$\frac{1}{P_r}\left(\Theta'' + \frac{\Theta'}{(\zeta + R_c)}\right) + \left(\frac{R_c}{(\zeta + R_c)}g\Theta' + N_t\Theta'^2 + N_b\Theta'\Phi' + \Gamma\Theta\right) = 0, \tag{11}$$

$$\frac{1}{L_e}\left(\Phi'' + \frac{\Phi'}{(\zeta + R_c)}\right) + \frac{R_c}{(\zeta + R_c)}g\Phi' + \frac{N_t}{L_e N_b}\left(\Theta'' + \frac{\Theta'}{(\zeta + R_c)}\right) - \varepsilon_1(1 + \varepsilon_2\Theta)^m \operatorname{Exp}\left(\frac{-E_1}{1 + \varepsilon_2\Theta}\right)\Phi = 0, \tag{12}$$

$$\frac{1}{L_b}\left(\Psi''+\frac{\Psi'}{(\zeta+R_c)}\right)+\frac{R_c}{(\zeta+R_c)}g\,\Psi'-\frac{P_e}{L_b}\left(\delta_1\Phi''+g\,\Phi''+g'\Phi'\right)=0, \tag{13}$$

where, $\alpha\left(=1/\rho_f\nu_1 Ba\right)$ and $\beta\left(=c^2b_1^3/6\nu_1a^2\right)$ symbolize the dimensionless Eyring-Powell fluid parameters, $P_e\left(=W_a b_a/D_n\right)$ the Peclet number, $R_c\left(=R_\alpha\sqrt{b_1/\nu_1}\right)$ the radius of curvature, $\delta_1\left(=N_\infty/\left(N_w-N_\infty\right)\right)$ the microorganism's difference parameter, $P_r\left(=\nu_1/\kappa\right)$ the Prandtl number, $\gamma\left(=(1-C_\infty)B_1^*g^*\left(T_w-T_\infty\right)/b_1^2c\right)$ the mixed convective parameter, $L_e\left(=\nu_1/D_\beta\right)$ the Lewis number, $\Gamma\left(=Q_0/b_1\rho_f c_{1f}\right)$ the heat production parameter, $\varepsilon_2\left(=\left(T_w-T_\infty\right)/T_\infty\right)$ the temperature difference variable, $Nr\left(=\left(\rho_f-\rho_f\right)\left(C_w-C_\infty\right)/(1-C_\infty)\left(T_w-t_\infty\right)\rho_f B_1^*\right)$ the buoyancy fraction variable, $N_t\left(=D_T\tau_\alpha\left(T_w-T_\infty\right)/\nu_1T_\infty\right)$ the nondimensional thermophoretic variable, $\varepsilon_1=\left(k_r^2/b_1\right)$ the reaction rate parameter, $L_b\left(=\nu_1/D_n\right)$ the bioconvection Lewis number, $N_b\left(=D_\beta\tau_\alpha\left(C_w-C_\infty\right)/\nu_1\right)$ the parameter of Brownian movement, $M\left(=\sigma M_0^2/\rho_f\,b_1\right)$ the magnetic parameter, $R_b\left(=\left(N_w-N_\infty\right)\gamma^*g^*\left(\rho_n-\rho_f\right)/\rho_f(1-C_\infty)B_1^*\left(T_w-T_\infty\right)\right)$ the bioconvection Rayleigh number, and $E_1=\left(-E_a/\chi T_\infty\right)$ the activation energy variable respectively.

After the exclusion of P from Eqs. (9) and (10), we have accomplished

$$\begin{aligned}&(1+\alpha)\left(g^{iv}+\frac{2g'''}{(R_c+\zeta)}-\frac{g''}{(R_c+\zeta)^2}+\frac{g'}{(R_c+\zeta)^3}\right)+\gamma\left(\Theta'+\frac{\Theta}{(R_c+\zeta)}\right)-\gamma\left(\Phi'+\frac{\Phi}{(R_c+\zeta)}\right)N_r\\&-\gamma\left(\Psi'+\frac{\Psi}{(R_c+\zeta)}\right)R_b-M^2\left(g''+\frac{g'}{(R_c+\zeta)}\right)+\frac{R_c}{(R_c+\zeta)}\left(g\,g'''-g'\,g''\right)-\frac{R_c g'^2}{(\zeta+R_c)^2}+\frac{R_c g\,g''}{(\zeta+R_c)^2}\\&-\frac{R_c g\,g'}{(\zeta+R_c)^3}-\alpha\beta\left(\begin{array}{l}3g''^2g^{iv}+6g''g'''^2+\frac{12g'g''g'''}{(\zeta+R_c)^2}+\frac{3}{(\zeta+R_c)^2}g''^3-\frac{9g'g''^2}{(\zeta+R_c)^3}+\frac{3g'^2g^{iv}}{(\zeta+R_c)^2}\\-\frac{6g'^2g'''}{(\zeta+R_c)^2}+\frac{9g'^2g''}{(\zeta+R_c)^4}-\frac{3g'^3}{(\zeta+R_c)^5}-\frac{6g^{iv}g'g''}{(\zeta+R_c)}-\frac{6g'g'''^2}{(\zeta+R_c)}-\frac{6g'''g''^2}{(\zeta+R_c)}\end{array}\right),\end{aligned} \tag{14}$$

With transmuted boundary conditions

$$\begin{aligned}&g(0)=0,\ \Psi(0)=1,\ 1=g'(0),\ \Phi(0)=1,\ \Theta(0)=1,\\&g'(\infty)=0,\ \Psi(\infty)=0,\ \Phi(\infty)=0,\ g''(\infty)=0,\ \Theta(\infty)=0.\end{aligned} \tag{15}$$

The physical quantities relevant to engineering and physical applications perspective are given as follows:

$$C_g=\frac{\tau_{rc}}{\rho_f u_w^2},\ \ Nu_c=\frac{c\,q_w}{(T_w-T_\infty)\kappa},\ \ Sh_c=\frac{c\,j_w}{(C_w-C_\infty)D_\beta},\ \ Mn_s=\frac{cq_n}{D_n\left(N_w-N_\infty\right)}, \tag{16}$$

here, τ_{rc}, q_n, q_w, and j_w are depicted by

$$\tau_{rc}=\left[\left(\mu+\frac{1}{Ba}\right)\left(\frac{\partial v}{\partial r}-\frac{v}{R_\alpha+r}\right)-\frac{1}{6\rho Ba^3}\left(\begin{array}{l}\left(\frac{\partial v}{\partial r}\right)^3-\frac{v^3}{\left(R_\alpha+r\right)^3}-\frac{3v}{\left(R_\alpha+r\right)}\left(\frac{\partial v}{\partial r}\right)^2\\+\frac{3v^2}{\left(R_\alpha+r\right)^2}\left(\frac{\partial v}{\partial r}\right)\end{array}\right)\right]_{\bar{r}=0},$$

$$q_w=-\left(\kappa\frac{\partial T}{\partial r}\right)\Bigg|_{r=0},\ j_w=-\left(D_\beta\frac{\partial C^*}{\partial r}\right)\Bigg|_{r=0},\ q_n=-\left(D_n\frac{\partial N^*}{\partial r}\right)\Bigg|_{r=0}. \tag{17}$$

By incorporating Eq. (8) in Eqs. (16) and (17), we get

$$Re_c^{1/2}C_g=\left[\left(1+\alpha\right)\left(g''(0)-\frac{1}{R_c}\right)-\alpha\beta\left(g'''(0)-\frac{1}{R_c^{\,3}}-\frac{3g''^2(0)}{R_c}+\frac{3g''(0)}{R_c^{\,2}}\right)\right]_{\bar{r}=0}, \tag{18}$$

$$Re_c^{-1/2}Nu_c=-\Theta'(0), \tag{19}$$

$$Re_c^{-1/2}Sh_c=-\Phi'(0), \tag{20}$$

$$Re_c^{-1/2}Mn_c=-\Psi'(0). \tag{21}$$

3. Entropy Generation

The entropy creation rate in dimensional form for the magnetized Eyring-Powell nanofluid flow containing microorganisms can be characterized as [48]

$$\begin{aligned}S_E=&\frac{\kappa}{T_\infty^2}\left(\frac{\partial T}{\partial r}\right)^2+\frac{\mu}{T_\infty}\left(\frac{\partial v}{\partial r}+\frac{v}{\left(R_\alpha+r\right)}\right)^2+\frac{\sigma M_0^2v^2}{T_\infty}+\frac{D_\beta}{C_\infty}\left(\frac{\partial C^*}{\partial r}\right)^2+\frac{D_\beta}{T_\infty}\left(\frac{\partial C^*}{\partial r}\frac{\partial T}{\partial r}\right)\\&\frac{D_n}{T_\infty}\left(\frac{\partial N^*}{\partial r}\frac{\partial T}{\partial r}\right)+\frac{D_n}{N_\infty}\left(\frac{\partial N^*}{\partial r}\right)^2,\end{aligned} \tag{22}$$

Applying Eq. (8), the non-dimensional form of Eq. (22) is

$$\begin{aligned}N_G=&\varepsilon_2\Theta'^2(\zeta)+M^2B_rg'^2+\delta_2\Theta'\Phi'+\frac{\delta_2\varepsilon_3}{\varepsilon_2}\Phi'^2+\frac{\delta_3}{\varepsilon_2\delta_1}\Psi'^2+\delta_3\Theta'\Psi'\\&+B_r\left(g''(\zeta)+\frac{g'(\zeta)}{\left(\zeta+R_c\right)}\right)^2,\end{aligned} \tag{23}$$

Where, $N_G\left(=\nu_1 T_\infty S_E/\kappa(T_w-T_\infty)b_1\right)$ represents the entropy production rate, $\varepsilon_3\left(=\left(C_w-C_\infty\right)/C_\infty\right)$ the nanoparticles concentration difference parameter, $\delta_2\left(=D_B\left(C_w-C_\infty\right)/\kappa\right)$ the non-dimensional nanoparticles diffusion constant, $\delta_3\left(=D_n\left(N_w-N_\infty\right)/\kappa\right)$ the non-dimensional microorganism's diffusion constant, and $B_r\left(=\mu b_1^2 c^2/\left(T_w-T_\infty\right)\kappa\right)$ the Brinkman number.

The dimensionless Bejan number is designated as

$$Be=\frac{\text{concentration irreversbility+heat transfer irreversibility+gyrotactic irreversibility}}{\text{Total irreversibility}}, \tag{24}$$

$$Be=\frac{\varepsilon_2\Theta'^2(\zeta)+\delta_2\Theta'\Phi'+\frac{\delta_2\varepsilon_3}{\varepsilon_2}\Phi'^2+\frac{\delta_3}{\varepsilon_2\delta_1}\Psi'^2+\delta_3\Theta'\Psi'}{\left(\varepsilon_2\Theta'^2(\zeta)+M^2B_r g'^2+\delta_2\Theta'\Phi'+\frac{\delta_2\varepsilon_3}{\varepsilon_2}\Phi'^2+\frac{\delta_3}{\varepsilon_2\delta_1}\Psi'^2+B_r\left(g''(\zeta)+\frac{g'(\zeta)}{(\zeta+R_c)}\right)^2+\delta_3\Theta'\Psi'\right)}, \tag{25}$$

4. Explanation of Shooting method

The nonlinear differential Eqs. (11), (12), (13), (14), and boundary conditions Eq. (15) are solved numerically through the Shooting technique. To implement this technique, the ordinary differential equations are first transmuted into a system of first-order ordinary differential equations by establishing new independent variables as

$$g'(\zeta)=p_1(\zeta),\ g''(\zeta)=q(\zeta),\ g'''=s(\zeta),\ \Theta'(\zeta)=t,\ \Phi'(\zeta)=u(\zeta),\ \Psi'(\zeta)=z(\zeta), \tag{26}$$

By employing Eq. (26), the nonlinear ODEs (11), (12), (13), (14), and boundary conditions Eq. (15) are stated as

$$\begin{aligned}
&\left((1+\alpha)-\alpha\beta\left(3q^2+\frac{3p_1^2}{(\zeta+R_c)^2}-\frac{6p_1q}{(\zeta+R_c)}\right)\right)s'=(1+\alpha)\left(\frac{q}{(R_c+\zeta)^2}-\frac{p_1}{(R_c+\zeta)^3}\right)\\
&-\gamma\left(t+\frac{\Theta}{(R_c+\zeta)}\right)+\gamma\left(u+\frac{\Phi}{(R_c+\zeta)}\right)N_r+\gamma\left(z+\frac{\Psi}{(R_c+\zeta)}\right)R_b+M^2\left(q+\frac{p_1}{(R_c+\zeta)}\right)\\
&-\frac{R_c}{(R_c+\zeta)}(g\,s+p_1q)+\frac{R_c p_1^2}{(\zeta+R_c)^2}-\frac{R_c g\,q}{(\zeta+R_c)^2}+\frac{R_c g\,p_1}{(\zeta+R_c)^3}\\
&+\alpha\beta\left(\begin{array}{l}6qs^2+\frac{12p_1qs}{(\zeta+R_c)^2}+\frac{3q^3}{(\zeta+R_c)^2}-\frac{9p_1q^2}{(\zeta+R_c)^3}-\frac{6p_1^2s}{(\zeta+R_c)^3}+\frac{9p_1^2q}{(\zeta+R_c)^4}\\-\frac{3p_1^3}{(\zeta+R_c)^5}-\frac{6p_1s^2}{(\zeta+R_c)}-\frac{6sq^2}{(\zeta+R_c)}\end{array}\right),
\end{aligned} \tag{27}$$

$$t' = -\frac{t}{(R_c+\zeta)} - \frac{P_r\, t\, g}{(R_c+\zeta)} - P_r N_b t u - P_r N_t t^2 - P_r \Gamma \theta, \tag{28}$$

$$u' = -\frac{u}{(R_c+\zeta)} - \frac{L_e\, u\, g}{(R_c+\zeta)} - \frac{N_t}{N_b}\left(t' + \frac{t}{(R_c+\zeta)}\right) + \varepsilon_1 (1+\varepsilon_2 \Theta)^m \exp\left(\frac{-E_1}{(1+\varepsilon_2\Theta)}\right)\Phi, \tag{29}$$

$$z' = -\frac{z}{(R_c+\zeta)} - \frac{L_b\, z\, g}{(R_c+\zeta)} + P_e\left(\delta_1 z' + g\, z' + t u\right), \tag{30}$$

Transmuted bcs

$$\begin{aligned} &g(0)=0,\ \Psi(0)=1,\ p_1(0)=1,\ \Phi(0)=1,\ \Theta(0)=1, \\ &p_1(\infty)=0,\ \Psi(\infty)=0,\ \Phi(\infty)=0,\ q(\infty)=0,\ \Theta(\infty)=0. \end{aligned} \tag{31}$$

The above resulting initial value problem is solved using a standard Runge–Kutta scheme, while the unknown initial conditions are iteratively adjusted to satisfy the boundary conditions at infinity. Convergence is ensured by minimizing the residual errors at the far-field boundary. The distinctive advantage of the Shooting method lies in its ability to efficiently handle strongly nonlinear, coupled boundary-layer equations without requiring spatial discretization or large matrix formulations, as is common in finite difference or finite element methods. This approach significantly reduces computational complexity and memory requirements. Moreover, the Shooting technique provides high numerical accuracy and smooth convergence at the asymptotic boundary, which is crucial for reliably capturing velocity, temperature, concentration, bioconvective, and entropy profiles. Additionally, the method offers direct control over asymptotic boundary conditions, making it particularly suitable for curved stretching geometries involving non-Newtonian fluids with complex transport phenomena. Due to these advantages, the Shooting technique has been widely adopted and proven reliable for similar nonlinear transport problems in the literature.

5. Discussions

The foremost intention of this part is to illuminate the key findings concerning the influence of divergent involved flow parameters, specifically the Eyring-Powell fluid parameters (α) and (β), activation energy parameter (E_1), bioconvection Lewis number (L_b), heat production parameter (Γ), radius of curvature parameter (R_c), nanoparticles concentration difference parameter (ε_3), buoyancy fraction variable (N_r), thermophoretic constant (N_t), nanoparticles diffusion constant (δ_2), reaction rate parameter (ε_1), microorganisms difference parameter (δ_1), Prandtl number (P_r), fitted rate parameter (m), temperature difference parameter (ε_2), Lewis number (L_e), mixed convective parameter (γ), Brownian motion variable (N_b), magnetic parameter (M), Peclet number (P_e), bioconvection Rayleigh number (R_b), microorganisms diffusion constant (δ_3), and the Brinkman number (B_r). Their impacts on the liquid velocity field, microorganisms and nanoparticles concentration fields,

temperature field, local Motile number, the local Sherwood number, entropy production profile, Nusselt numbers, Bejan number, and coefficient of skin friction are determined via graphical and tabular representations.

Table 1 presents a comparison of the skin friction coefficient with previously published results of Imran and Naveed [4], Haq et al. [10], and Kumar et al. [15], to validate the accuracy of the present numerical scheme under the limiting case. The obtained numerical values show an appreciable agreement with the available literature, confirming the correctness of the mathematical formulation and numerical implementation. This close correspondence validates the reliability and robustness of the present model and solution methodology.

Table 2 is arranged to describe the variation in the magnitude of the local Sherwood number due to the impacts of various parameters, specifically (N_t), (R_c), (ε_1), (L_e), (N_b), (ε_2), (m), and (E_1). We have concluded that the magnitude of the Sherwood number is heightened for larger values of (N_t), (L_e), (ε_1), (ε_2), and (m). While for upward values of (R_c), (N_b), and (E_1), it decreases. Physically, higher thermophoretic forces intensify the transport of nanoparticles from the heated surface toward the cooler regions, whereas the mathematical relation of the Lewis number indicates that larger values suppress mass diffusivity. Both mechanisms enhance the nanoparticle concentration gradient at the wall. Furthermore, improved values of the reaction rate and fitted rate parameters strengthen the activation-energy-controlled chemical reaction near the surface, causing a greater reduction in nanoparticle concentration and a noticeable increase in the concentration gradient, which ultimately augments the Sherwood number.

Table 3 exposes the numerical results for the local Motile number $\mathrm{Re}_c^{-1/2} M n_c$ under the stimuli of (R_c), (L_b), (δ_1), and (P_e). The magnitude of the Motile number reduces with advanced values of the curvature variable (R_c) and it increases with (L_b), (δ_1) and (P_e). The local Motile number quantifies the transport and concentration of motile microorganisms in the nanofluid. An enhancement in the radius of curvature effectively expands the flow region, weakening the convective transport of microorganisms along the surface and thereby diminishing the local Motile number. Conversely, higher Peclet numbers enhance chemotaxis-driven transport relative to microorganism diffusion, promoting stronger microorganism migration toward the surface and enhancing the Motile number. Similarly, larger values of the microorganism difference parameter amplify concentration gradients, leading to enhanced microorganism density near the surface and a corresponding rise in the Motile number. Furthermore, an increase in the bioconvective Lewis number, which signifies reduced microorganism diffusivity relative to momentum diffusion, restricts the spreading of microorganisms and causes their accumulation near the wall, and as a result, an enhancement in the magnitude of the local Motile number is noticed.

Figure 2 (a-e) illustrates the variation in the liquid velocity profile $g'(\zeta)$ under the influence of (α), (β), (γ), (N_r), (R_b), and (M). This graph reveals that the velocity profile boosts up with developing values of (α), whereas it drops for all other specified parameters.

The change in the pressure field $P(\zeta)$ against upward values of (α), (β), (γ), (N_r), (R_b), and (M) is shown in Figure 3 (a-f). This figure demonstrates the positive trend in the pressure field as all variables are enhanced. The physical reason for the upward response of the pressure field with higher values of the Eyring-Powell fluid parameters is that the resistance of fluid particles increases, which reduces the deformation rate and consequently leads to a rise in the magnitude of the pressure field. Similarly, higher values of the bioconvection Rayleigh number, mixed convective parameter, and buoyancy fraction parameter enhance buoyancy-driven motion and density-driven forces, intensifying fluid flow near the surface and consequently increasing the pressure field. Additionally, the magnetic parameter generates a Lorentz force that opposes fluid motion, contributing to higher pressure within the boundary layer.

Figure 4 (a-d) interprets the consequences of (R_c), (P_r), (N_b), (Γ), and (N_t) on temperature distribution $\Theta(\zeta)$. The profile $\Theta(\zeta)$ show a contrary response against growing values of (R_c), and (P_r) (see Figures 4(a), 4(c)). Figures 4(b) and (d) perceived that the temperature profile shows a favorable response for increasing values of (N_b), (Γ), and (N_t). An enhancement in the temperature profile is observed for higher values of the thermophoresis parameter, Brownian motion parameter, and heat generation parameter, as these mechanisms improve energy transport within the fluid. As the thermophoresis parameter rises, nanoparticles transport thermal energy more efficiently from hotter to cooler regions, leading to an increase in fluid temperature. Higher values of the Brownian motion parameter intensify the random motion resulting from collisions between nanoparticles and the base fluid, which promotes thermal diffusion and elevates the temperature. Additionally, an increased heat production parameter directly distributes energy to the system, further raising the temperature profile throughout the boundary layer.

Figure 5 (a-d) is organized to explicate the significance of dissimilar variables, particularly the activation energy parameter (E_1), temperature difference parameter (ε_2), Lewis number (L_e), the reaction rate parameter (ε_1), and fitted rate parameter (m) on the nanoparticle concentration distribution $\Phi(\zeta)$. An enhancement in the magnitude of $\Phi(\zeta)$ is noticed due to the altered values of the activation energy parameter (E_1), while the magnitude of $\Phi(\zeta)$ declines for the escalated values of all the other stated parameters. An enhancement in the magnitude of nanoparticle concentration with the activation energy parameter is observed because higher values of activation energy slow down the chemical reaction at the surface. Consequently, the movement of nanoparticles by the reaction is reduced, allowing more nanoparticles to accumulate near the surface, thereby increasing the concentration.

Figure 6 (a-d) depicts the variation in the magnitude of the microorganism concentration field $\Psi(\zeta)$ because of the mounting values of (R_c), (δ_1), (L_b), and (P_e). It can be determined that as the values of all the parameters incline, the magnitude of $\Psi(\zeta)$ gradually reduces. The reduction in the microorganism concentration field with increasing Peclet number and bioconvective Lewis number arises from their effect on microorganism diffusivity. Mathematically, a higher Peclet number indicates stronger chemotaxis-driven transport relative to microorganism diffusion, which thins the concentration boundary layer near the surface and decreases the microorganism concentration. Similarly, the bioconvective Lewis number signifies the ratio of momentum diffusion to microorganism diffusion. Larger values of the bioconvective Lewis number suggest lower microorganism diffusivity relative to fluid momentum, controlling microorganism transport and consequently reducing their concentration near the surface.

Figure 7(a-c) illustrates the stimulus of (R_c) versus (M), (α) versus (β), and (R_b) versus (γ) on skin friction coefficient $\left(\sqrt{\mathrm{Re}_c}C_g\right)$. This graph witnesses that the magnitude of skin friction is an increasing function of (R_c), (α), (β), and (γ). However, the magnitude of skin friction drops gradually against higher values of (M) and (R_b).

Figure 8 (a-b) is plotted to explore the alteration in the local Nusselt number $\left(Nu_c/\sqrt{\mathrm{Re}_c}\right)$ magnitude under the influence of (Γ) vs (P_r) and (N_t) versus (N_b). This graph clarifies that the magnitude of $\left(Nu_c/\sqrt{\mathrm{Re}_c}\right)$ shows opposite behavior for all defined variables.

Figure 9 (a-b) explains the consequences of (B_r), (R_c), (ε_2), and (M) on the entropy production field $N_G(\zeta)$. A growing response in the magnitude of $N_G(\zeta)$ is observed against all defined variables.

Figure 10 (a-c) is plotted to determine the effects of (B_r), (R_c), (δ_1), (ε_3), (δ_2), and (M) on Bejan number $Be(\zeta)$. The magnitude of the Bejan number is a reducing function of the parameters (B_r), (R_c), (δ_1), and (M). However, for upward values of (ε_3) and (δ_2), its magnitude exhibits a developing trend.

6. Operational Interpretation and Case Based Recommendation

From an operational standpoint, the parametric results may be subdivided into different modes of working based on the required transport performance. For applications where enhanced nanoparticle mass transfer is required (e.g., catalytic surface transport or biothermal processing), higher values of the thermophoretic parameter and Lewis number are beneficial because they strengthen mass diffusion toward the surface, resulting in a noticeable increase in

the Sherwood number. Conversely, if uniform microorganism distribution and bioconvective enhancement are desired (e.g., in microbial bioreactors and oxygenation systems), the preferable operating regime involves a higher Peclet number and bioconvection Lewis number, as chemotaxis-driven transport dominates over diffusive spreading, thereby increasing the motile microorganism concentration near the wall. In contrast, an increase in the radius of curvature parameter weakens both nanoparticle and microorganism transport, indicating that geometries with smaller curvature provide more favorable conditions for combined thermal and bioconvective performance. Furthermore, entropy generation increases under stronger viscous and magnetic irreversibilities, implying that systems requiring high thermodynamic efficiency should be operated at lower Brinkman number and magnetic parameter. These operational interpretations connect the individual parametric influences into unified working scenarios and provide guidance on how the system may be adjusted according to performance demands.

7. Conclusions

The key objective of this theoretical research is to analyze the significant effects of gyrotactic microorganisms and activation energy on the bioconvective flow of an Eyring-Powell nanofluid on a curvy stretchable surface. In addition, the roles of thermophoretic and Brownian diffusion, along with entropy generation, are thoroughly examined. Numerical solutions are obtained for the system of governing flow equations to illustrate the physical behavior of the model.

The primary results of the current study are as follows:

- Fluid velocity rises with rising values of the Eyring-Powell fluid parameter (α), whilst it drops for improving values of bioconvection Rayleigh number, mixed convective difference parameter, buoyancy fraction variable, Eyring-Powell fluid parameter (β), and the magnetic parameter.
- Pressure distribution of liquid depicts a positive trend against higher values of Eyring-Powell fluid parameters, bioconvection Rayleigh number, mixed convective parameter, buoyancy fraction variable, and magnetic parameter.
- Temperature distribution develops with the growth of the thermophoretic constant, heat production parameter, and Brownian motion variable. However, it reduces when the parameter of radius of curvature and Prandtl number are mounted.
- Magnitude of the concentration field grows when the values of the activation energy parameter are inclined, and for mounting values of the reaction rate parameter, Lewis number, temperature difference parameter, and fitted rate parameter, its magnitude shows a contrary response.

- Magnitude of the microorganism concentration field shows a contrary response for upsurge values of the Peclet number, microorganisms difference parameter, bioconvection Lewis number, and radius of curvature parameter.
- Skin friction coefficient magnitude declines when an increment in bioconvection Rayleigh number and magnetic parameter occurs. Whereas for improved values of Eyring-Powell fluid parameters, mixed convective difference parameter, and radius of curvature, it increases.
- The Sherwood number is found to increase appreciably with the thermophoretic parameter and the Lewis number. For instance, increasing the thermophoretic parameter from 0.1 to 0.9 enhanced the Sherwood number by approximately 21%, while increasing the Lewis number from 0.5 to 2.5 improved the Sherwood number by nearly 23%, indicating stronger nanoparticle mass transfer due to reduced mass diffusivity and enhanced thermophoretic transport. In contrast, the radius of curvature parameter suppressed nanoparticle transport; increasing the radius of curvature from 2.0 to 4.5 reduced the Sherwood number by about 6%, demonstrating that the radius of curvature parameter weakens concentration gradients along the boundary layer.
- Entropy production field enhances with upward values of Brinkman number, radius of curvature parameter, temperature difference parameter, and magnetic parameter.
- Magnitude of local Bejan number exhibits a mounting trend with developing values of nanoparticles concentration difference parameter and nanoparticles diffusion constant. While the Bejan number magnitude reduces with uphill values of the Brinkman number, radius of curvature parameter, microorganisms difference parameter, and magnetic parameter.
- An increase in Peclet number from 0.1 to 0.7 resulted in an enhancement in the magnitude of Motile number of approximately 42%, while increasing bioconvection Lewis number from 0.5 to 3.5 increased the magnitude of Motile number by roughly 18%, confirming that chemotaxis-driven bioconvective motion dominates diffusion-driven spreading. Conversely, increasing the radius of curvature parameter weakened microorganism transport, where the Motile number decreased by nearly 8% as the radius of curvature increased from 2.0 to 4.5.

The key findings of this novel study provide essential insights for the optimization and design of thermal systems involving non-Newtonian nanofluids, particularly in curved stretching geometries with microorganism-induced bioconvection and activation energy effects. Enhanced nanoparticle transport, heat transfer, and controlled microorganism concentration can be applied in bioengineering systems, bioreactors, electronic cooling, polymer extrusion, catalytic reactors, and chemical processing units. Future research may extend the model to unsteady flows, hybrid nanofluids, ternary hybrid nanofluids, thermal radiation effects, variable thermophysical properties, and more complex chemical reactions. Quantitatively, the study highlights that nanoparticle concentration rises notably with increasing activation energy, while the magnitude of skin friction and entropy generation are strongly influenced by fluid parameters, magnetic field strength, and radius of curvature, providing precise benchmarks for engineering and industrial applications.

Acknowledgment: We are thankful to the honorable reviewers for their encouraging comments and constructive suggestions to improve the quality of the manuscript.

References

[1] Sajid, M., Ali, N., Javed, T., et al. "Stretching a curved surface in a viscous fluid", Chinese Physics Letters, **27**(2), pp. 024703 (2010). https://doi.org/10.1088/0256-307X/27/2/024703

[2] Shabbir, T., Mushtaq, M., Khan, M. I., et al. "Modeling and numerical simulation of micropolar fluid over a curved surface: Keller box method", Computer methods and programs in biomedicine, **187**, pp. 105220 (2020). https://doi.org/10.1016/j.cmpb.2019.105220

[3] Ahmed, K., Akbar, T., Muhammad, T., et al. "Heat transfer characteristics of MHD flow of Williamson nanofluid over an exponential permeable stretching curved surface with variable thermal conductivity", Case Studies in Thermal Engineering, **28**, pp. 101544 (2021). https://doi.org/10.1016/j.csite.2021.101544

[4] Imran, M., Naveed, M., "Analysis of thermophoretic and Brownian diffusions in hydromagnetic curvilinear flow of Carreau nanofluid with activation energy and heat generation", Results in Engineering, **24**, pp. 103114 (2024). https://doi.org/10.1016/j.rineng.2024.103114

[5] Naveed, M., Imran, M., Khadim, F., "Dynamics of chemical reactions and temperature-dependent thermal conductivity in a viscous fluid over an oscillating curved surface", Science Progress, **108**(2), pp. 00368504251343498 (2025). https://doi.org/10.1177/00368504251343498

[6] Qian, W. M., Khan, M. I., Shah, F., et al. "Mathematical modeling and MHD flow of micropolar fluid toward an exponential curved surface: heat analysis via ohmic heating and heat source/sink", Arabian Journal for Science and Engineering, **47**(1), pp. 867-878 (2022). https://doi.org/10.1007/s13369-021-05673-w

[7] Dinesh, P., Yadav, S., Jyothirmayi, M., "Nonlinear stretching curved surface and Lorentz force effect on hybrid nanofluids with an activation energy", International Journal of Thermofluids, **24**, pp. 100983 (2024). https://doi.org/10.1016/j.ijft.2024.100983

[8] Iqbal, J., Abbasi, F. M., Alam, M. M., "Non-similar analysis for magnetohydrodynamic flow of hybrid nanofluid over a curved stretching surface with hall current and viscous dissipation effects", Modern Physics Letters B, **39**(27), pp. 2550145 (2025). https://doi.org/10.1142/S0217984925501453

[9] Naveed, M., Imran, M., Abbas, Z., "Effect of Chemical Reaction on Bioconvective Flow of Gyrotactic Micro-organisms in Hybrid Nanofluid on a Curved Oscillating Surface with Thermal Radiation", Arabian Journal for Science and Engineering, **50**, pp. 20543–20562 (2025). https://doi.org/10.1007/s13369-025-10131-y

[10] Haq, S. U., Ashraf, M. B., Nawaz, R., "MHD flow of Carreau fluid over a curved stretching surface with Cattaneo–Christov heat flux model and chemical reaction", Numerical

Heat Transfer, Part B: Fundamentals, **86**(6), pp. 1583-1598 (2025). https://doi.org/10.1080/10407790.2024.2317922

[11] Khan, A. A., Saleem, I., Ellahi, R., et al. "On magnetohydrodynamics Powell–Eyring fluid with Cattaneo–Christov heat flux over a curved surface"; International Journal of Modern Physics B, **37**(19), pp. 2350190 (2023). https://doi.org/10.1142/S0217979223501904

[12] Naveed, M., Imran, M., Akhtar, S., et al. "Dynamics of melting heat transfer in thermally developed and chemically reactive flow of Eyring-Powell liquid through a curved channel", Ricerche di Matematica, **72**(1), pp. 299-316 (2023). https://doi.org/10.1007/s11587-021-00657-2

[13] Afridi, M. I., Mkhatshwa, M. P., Qasim, M., et al. "Thermal and computational analysis of MHD dissipative flow of Eyring–Powell fluid: Non-similar approach via overlapping grid-based spectral collocation scheme", Chinese Journal of Physics, **92**, pp. 1026-1042 (2024). https://doi.org/10.1016/j.cjph.2024.09.035

[14] Karthik, S., Iranian, D., Alhazmi, H., et al. "Double diffusive on Powell Eyring fluid flow by mixed convection from an exponential stretching surface with variable viscosity/thermal conductivity", Case Studies in Thermal Engineering, **55**, pp. 104091 (2024). https://doi.org/10.1016/j.csite.2024.104091

[15] Kumar, P., Vidhya, K. G., Almeida, F., et al. "Optimization using response surface methodology for Eyring-Powell fluid flow with Cattaneo-Christov heat flux and cross diffusion effects", International Journal of Thermofluids, **25**, pp. 100981 (2025). https://doi.org/10.1016/j.ijft.2024.100981

[16] Jafaripournimchahi, A., Shateri, A., Jalili, B., et al. "The effects of magnetic field and thermal radiation on the mixed convection of Al2O3-Cu/water hybrid nanofluid over a permeable vertical flat plate", Modern Physics Letters B, **38**(25), p.2450242 (2024). https://doi.org/10.1142/S0217984924502427

[17] Abbas, Z., Imran, M., Naveed, M., "Impact of equally diffusive chemical reaction on time-dependent flow of Casson nanofluid due to oscillatory curved stretching surface with thermal radiation", Arabian Journal for Science and Engineering, **47**(12), pp. 16059-16078 (2022). https://doi.org/10.1007/s13369-022-06792-8

[18] Nandeppanavar, M. M., Basha, H., Udgiri, S., "Buongiorno's radiative Prandtl-Eyring nanofluid flow through porous medium over a stretching surface with cross-diffusion effects", Proceedings of the Institution of Mechanical Engineers, Part N: Journal of Nanomaterials, Nanoengineering and Nanosystems, pp. 23977914241270753 (2024). https://doi.org/10.1177/23977914241270753

[19] Haq, S. U., Ashraf, M. B., Anjum, H. J., "Convective flow of Carreau fluid over a curved surface in presence of thermophoresis and Brownian motion", Waves in Random and Complex Media, **35**(2), pp. 3542-3556 (2025). https://doi.org/10.1080/17455030.2022.2053239

[20] Imran, M., Naveed, M., Rafiq, M. Y., et al. "Bio-convective flow of gyrotactic microorganisms in nanofluid through a curved oscillatory channel with Cattaneo-Christov double diffusion theory", Chinese Physics B, (2025). https://doi.org/10.1088/1674-1056/ade066

[21] Sheikholeslami, M., "Magnetic source impact on nanofluid heat transfer using CVFEM", Neural Computing and Applications, **30**(4), pp. 1055-1064 (2018). https://doi.org/10.1007/s00521-016-2740-7

[22] Sheikholeslami, M., "Numerical approach for MHD Al2O3-water nanofluid transportation inside a permeable medium using innovative computer method", Computer Methods in Applied Mechanics and Engineering, **344**, pp. 306-318 (2019). https://doi.org/10.1016/j.cma.2018.09.042

[23] Sheikholeslami, M., Ellahi, R., "Three-dimensional mesoscopic simulation of magnetic field effect on natural convection of nanofluid", International Journal of Heat and Mass Transfer, **89**, pp. 799-808 (2015). https://doi.org/10.1016/j.ijheatmasstransfer.2015.05.110

[24] Ali, B., Hussain, S., Shafique, M., et al. "Analyzing the interaction of hybrid base liquid C2H6O2–H2O with hybrid nano-material Ag–MoS2 for unsteady rotational flow referred to an elongated surface using modified Buongiorno's model: FEM simulation", Mathematics and Computers in Simulation, **190**, pp. 57-74 (2021). https://doi.org/10.1016/j.matcom.2021.05.012

[25] Ali, L., Wu, Y.J., Ali, B., et al. "The crucial features of aggregation in TiO2-water nanofluid aligned of chemically comprising microorganisms: A FEM approach", Computers & mathematics with applications, **123**, pp. 241-251 (2022). https://doi.org/10.1016/j.camwa.2022.08.028

[26] Sadiq, K., Jarad, F., Siddique, I., et al. "Soret and Radiation Effects on Mixture of Ethylene Glycol-Water (50%-50%) Based Maxwell Nanofluid Flow in an Upright Channel", Complexity, **2021**(1), p. 5927070 (2021). https://doi.org/10.1155/2021/5927070

[27] Li, C., Roshani, H., Jalili, M., et al. "Influence of hybrid nanofluids on entropy dynamics and transient thermal behavior in a finned enclosure with cylindrical obstruction", Case Studies in Thermal Engineering, **72**, pp.106339 (2025). https://doi.org/10.1016/j.csite.2025.106339

[28] Chari, F.N., Ganji, D.D., Mahboobtosi, M., et al. "Heat transfer analysis of GO/water nanofluid flow under the influence of Joule heating and chemical reactions with MHD: analytical and numerical concept", Multiscale and Multidisciplinary Modeling, Experiments and Design, **8**(5), pp. 264 (2025). https://doi.org/10.1007/s41939-025-00843-x

[29] Hajizadeh, S., Jalili, P., Jalili, B., et al. "A novel approach to investigate the effect of hybrid nanofluids in a non-Newtonian Maxwell model on thermal management for medical engineering applications", Modern Physics Letters B, **39**(28), pp. 2550140 (2025). https://doi.org/10.1142/S0217984925501404

[30] Hajizadeh, S., Jalili, P., Jalili, B., et al. “Innovative binary nanofluid approach with copper (Cu-EO) and Magnetite (Fe3O4-EO) for enhanced thermal performance”, Case Studies in Thermal Engineering, **63**, pp. 105191 (2024). https://doi.org/10.1016/j.csite.2024.105191

[31] Haider, S. M. A., Ali, B., Wang, Q., et al. “Stefan blowing impacts on unsteady mhd flow of nanofluid over a stretching sheet with electric field, thermal radiation and activation energy”, Coatings, **11**(9), p. 1048 (2021). https://doi.org/10.3390/coatings11091048

[32] Kumar, R. S. V., Alhadhrami, A., Gowda, R. J. P., et al. “Exploration of Arrhenius activation energy on hybrid nanofluid flow over a curved stretchable surface”, ZAMM-Journal of Applied Mathematics and Mechanics/Zeitschrift für Angewandte Mathematik und Mechanik, **101**(12), pp. e202100035 (2021). https://doi.org/10.1002/zamm.202100035

[33] Ali, B., Nie, Y., Hussain, S., et al. “Insight into the dynamics of fluid conveying tiny particles over a rotating surface subject to Cattaneo–Christov heat transfer, Coriolis force, and Arrhenius activation energy”, Computers & Mathematics with Applications, **93**, pp. 130-143 (2021). https://doi.org/10.1016/j.camwa.2021.04.006

[34] Ahmad, L., Khan, M., “Importance of activation energy in development of chemical covalent bonding in flow of Sisko magneto-nanofluids over a porous moving curved surface”, International Journal of Hydrogen Energy, **44**(21), pp. 10197-10206 (2019). https://doi.org/10.1016/j.ijhydene.2019.02.162

[35] Reddy, S. C., Asogwa, K. K., Yassen, M. F., et al. “Dynamics of MHD second-grade nanofluid flow with activation energy across a curved stretching surface”, Frontiers in Energy Research, **10**, pp. 1007159 (2022). https://doi.org/10.3389/fenrg.2022.1007159

[36] Sudarmozhi, K., Iranian, D., Alhazmi, H., et al. “Effect of heat generation and activation energy on MHD maxwell fluid with multiple slips”, Case Studies in Thermal Engineering, **59**, pp. 104424 (2024). https://doi.org/10.1016/j.csite.2024.104424

[37] Ahmed, F., E-Rabbi, S. R., Ali, M. Y., et al. “Numerical modeling of a MHD non-linear radiative Maxwell nano fluid with activation energy”, Heliyon, **10**(2), (2024). https://doi.org/10.1016/j.heliyon.2024.e24098

[38] Hayat, T., Ullah, I., Muhammad, K., et al, “Gyrotactic microorganism and bio-convection during flow of Prandtl-Eyring nanomaterial”, Nonlinear Engineering, **10**(1), pp. 201-212 (2021). https://doi.org/10.1515/nleng-2021-0015

[39] Rashed, A. S., Nasr, E. H., Mabrouk, S. M., “Influence of gyrotactic microorganisms on bioconvection in electromagnetohydrodynamic hybrid nanofluid through a permeable sheet”, Computation, **12**(1), pp. 17 (2024). https://doi.org/10.3390/computation12010017

[40] Sarma, A. K., Sarma, D., “Unsteady magnetohydrodynamic bioconvection Casson fluid flow in presence of gyrotactic microorganisms over a vertically stretched sheet”, Numerical Heat Transfer, Part A: Applications, pp. 1-24 (2024). https://doi.org/10.1080/10407782.2024.2389338

[41] Ahsan, N., Aslam, M. N., Khan, M. N., et al. “Bioconvective flow analysis of non-Newtonian fluid over a porous curved stretching surface”, Proceedings of the Institution of Mechanical Engineers, Part N: Journal of Nanomaterials, Nanoengineering and Nanosystems, pp. 23977914241231891 (2024). https://doi.org/10.1177/23977914241231891

[42] Hamid, A., Mehtab, U., Farooq, N., “Computational analysis for bioconvection flow of nanofluid along a bidirectional surface containing gyrotactic microorganisms embedded in a Darcy-Forchheimer porous medium”, International Journal of Thermofluids, **26**, pp. 101059 (2025). https://doi.org/10.1016/j.ijft.2025.101059

[43] Mahboobtosi, M., Ehsani, H., Ganji, A.M., et al. “AI-driven modeling of bioconvective nanofluid flow: An ANN approach to anisotropic slip and heat transfer in 3D systems”, International Communications in Heat and Mass Transfer, **165**, pp. 109035 (2025). https://doi.org/10.1016/j.icheatmasstransfer.2025.109035

[44] Shateri, A., Ganji, A.M., Jalili, P., et al. “Utilizing Python for numerical analysis of bioconvection in magnetized Casson-Maxwell nanofluid systems with gyrotactic microorganisms: An investigation of dominant factors”, Results in Engineering, **25**, pp. 103760 (2025). https://doi.org/10.1016/j.rineng.2024.103760

[45] Abdal, S., Mariam, A., Ali, B., et al. “Implications of bioconvection and activation energy on Reiner–Rivlin nanofluid transportation over a disk in rotation with partial slip”, Chinese Journal of Physics, **73**, pp. 672-683 (2021). https://doi.org/10.1016/j.cjph.2021.07.022

[46] Sadighi, S., Afshar, H., Jabbari, M., et al. “An analytical approach to entropy production in MHD mixed convection micropolar fluid flow over an inclined porous stretching sheet”, Frontiers in Mechanical Engineering, **8**, pp. 900316 (2022). https://doi.org/10.3389/fmech.2022.900316

[47] Swamy, H. A. K., Sankar, M., Reddy, N. K., et al. “Optimization of entropy generation and thermal mechanism of MHD hybrid nanoliquid flow in a sinusoidally heated porous cylindrical chamber”, Case Studies in Thermal Engineering, **51**, pp. 103615 (2023). https://doi.org/10.1016/j.csite.2023.103615

[48] Imran, M., Naveed, M., Rasheed, M. W., “Analysis of heat transfer in magnetized Williamson fluid over a porous curved oscillating surface: Entropy generation”, International Journal of Geometric Methods in Modern Physics, **22**(11), pp. 2550087 (2025). https://doi.org/10.1142/S0219887825500872

[49] Mandal, S., Mukherjee, S., Shit, G. C., et al. “Entropy analysis of MHD flow in hybrid nanofluid over a rotating disk with variable viscosity and nonlinear thermal radiation”, ZAMM-Journal of Applied Mathematics and Mechanics/Zeitschrift für Angewandte Mathematik und Mechanik, **105**(2), pp. e202301027 (2025). https://doi.org/10.1002/zamm.202301027

[50] Yazdi, M. H., Mahrooghi, A., Alatas, M., et al. “Entropy generation analysis of ferrofluid flow over horizontal surface with heat source and radiative effects”, Results in Engineering, **26**, pp. 105320 (2025). https://doi.org/10.1016/j.rineng.2025.105320

Biographies

Dr. Muhammad Imran is serving as an Assistant Professor in the Department of Mathematics, University of Education, Lahore, Pakistan. He obtained his Ph. D degree in Applied Mathematics. His primary research interests are in Fluid Mechanics, Heat and Mass Transfer analysis, Nanofluid flow, flow analysis on curved moving geometries, and Analytical and Numerical computations.

Dr. Muhammad Naveed is working as an Associate Professor in the Department of Mathematics, University of Education, Lahore, Pakistan. He earned Ph. D degree in Applied Mathematics. His research interests include Newtonian and non-Newtonian fluid flow, magnetohydrodynamics (MHD), Fluid Flow in Porous Medium, Heat and Mass Transfer, Nanofluid flow, flow on various shapes of curved geometries, Analytical and Numerical Solutions for ODEs and PDEs.

Fig. 1: Illustration of flow configuration

Fig. 2: Variations in $g'(\zeta)$.

Fig. 3: Variations in $P(\zeta)$.

Fig. 4: Variations in $\Theta(\zeta)$.

Fig. 5: Variations in $\Phi(\zeta)$.

Fig. 6: Variations in $\Psi(\zeta)$.

Fig. 7: Variations in $\sqrt{Re_x}C_g$.

Fig. 8: Variations in $Nu_x / \sqrt{Re_x}$.

Fig. 9: Variations in $N_G(\zeta)$.

Fig. 10: Variations in $Be(\zeta)$.

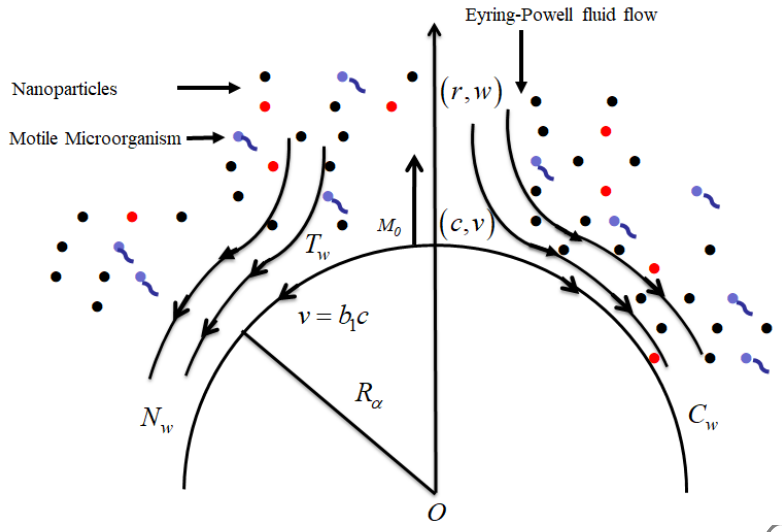

Fig. 1

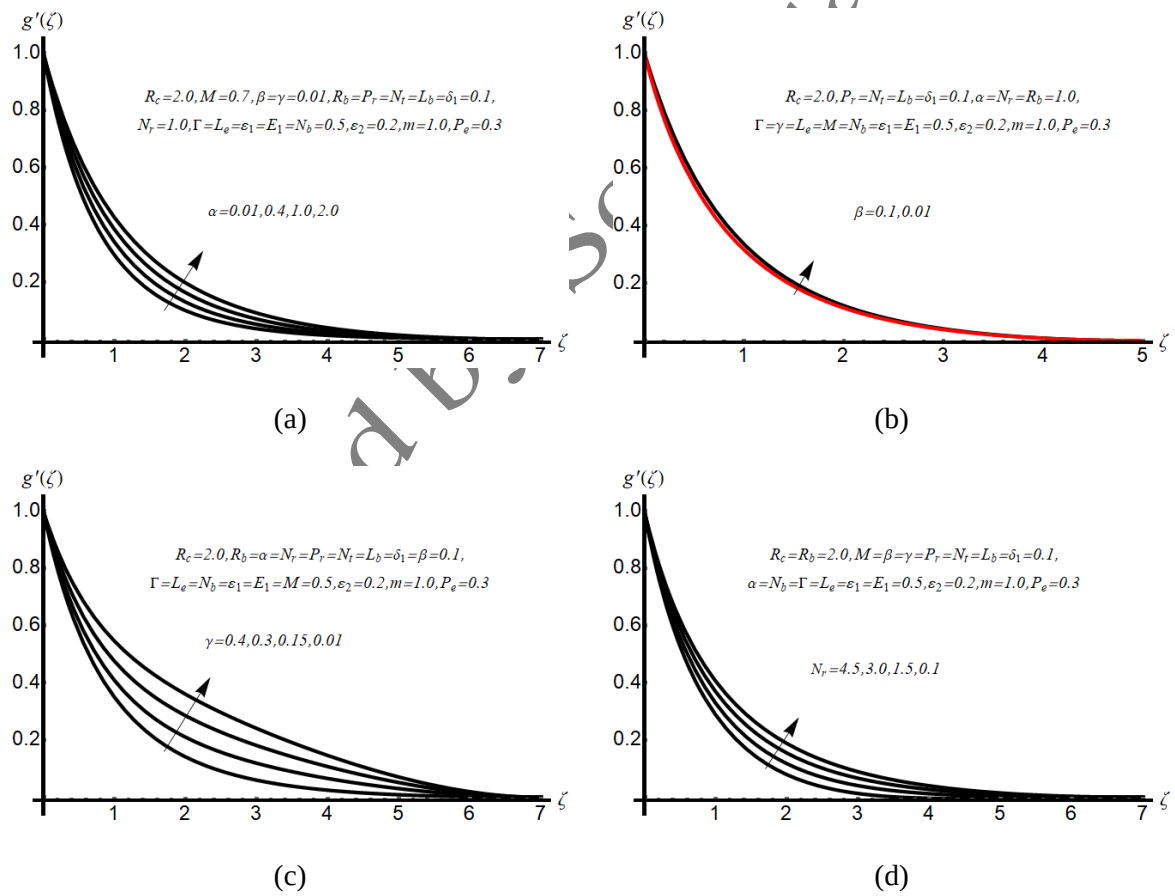

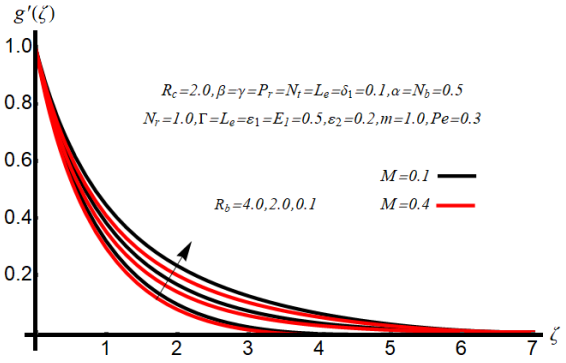

(e)

Fig. 2

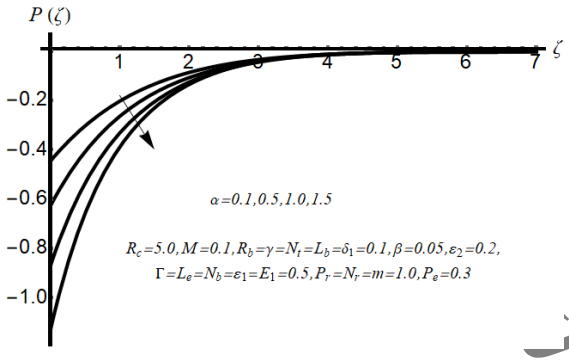

(a)

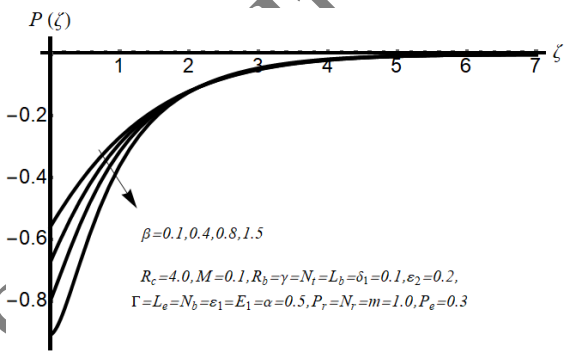

(b)

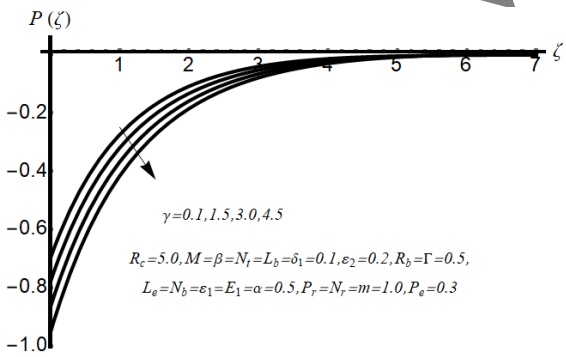

(c)

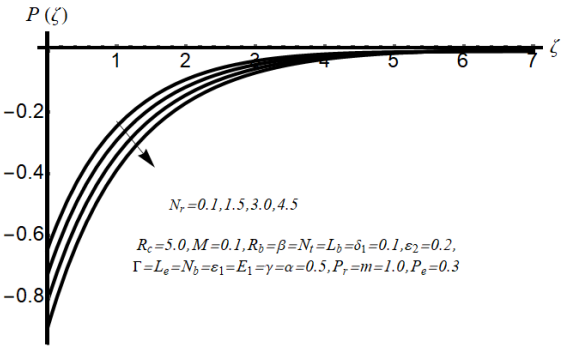

(d)

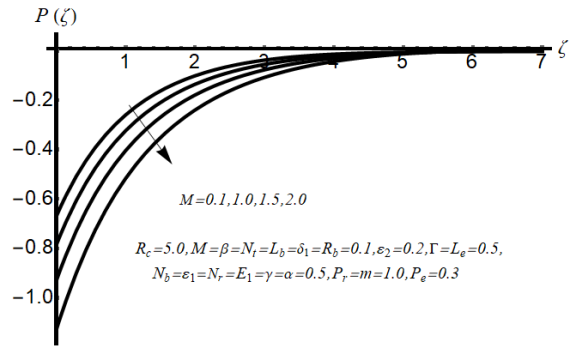

(e)

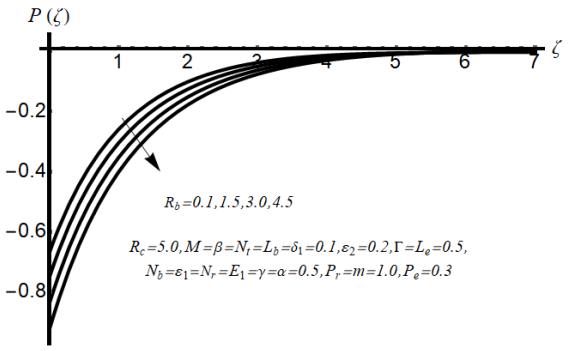

(f)

Fig. 3

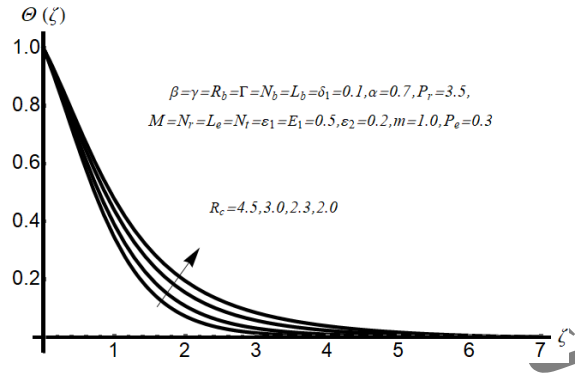

(a)

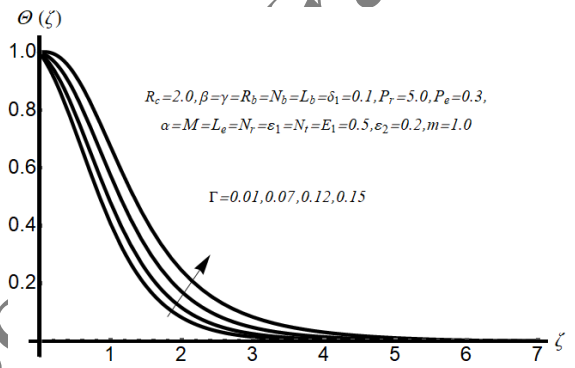

(b)

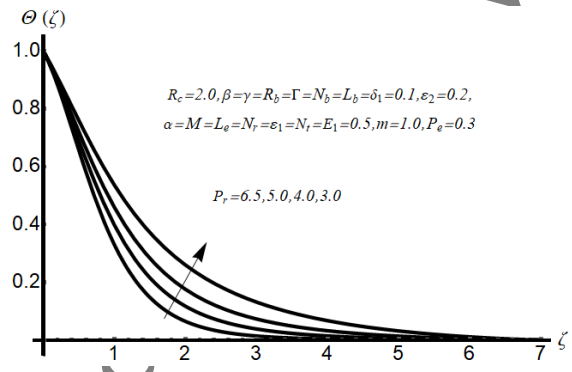

(c)

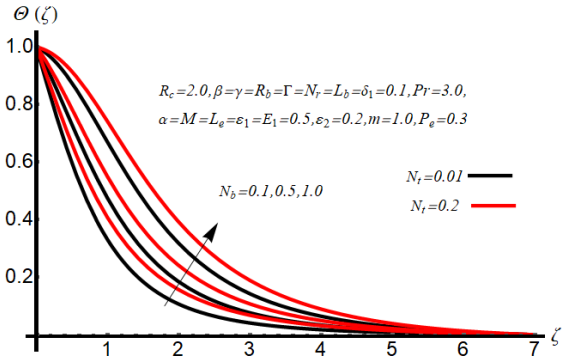

(d)

Fig. 4

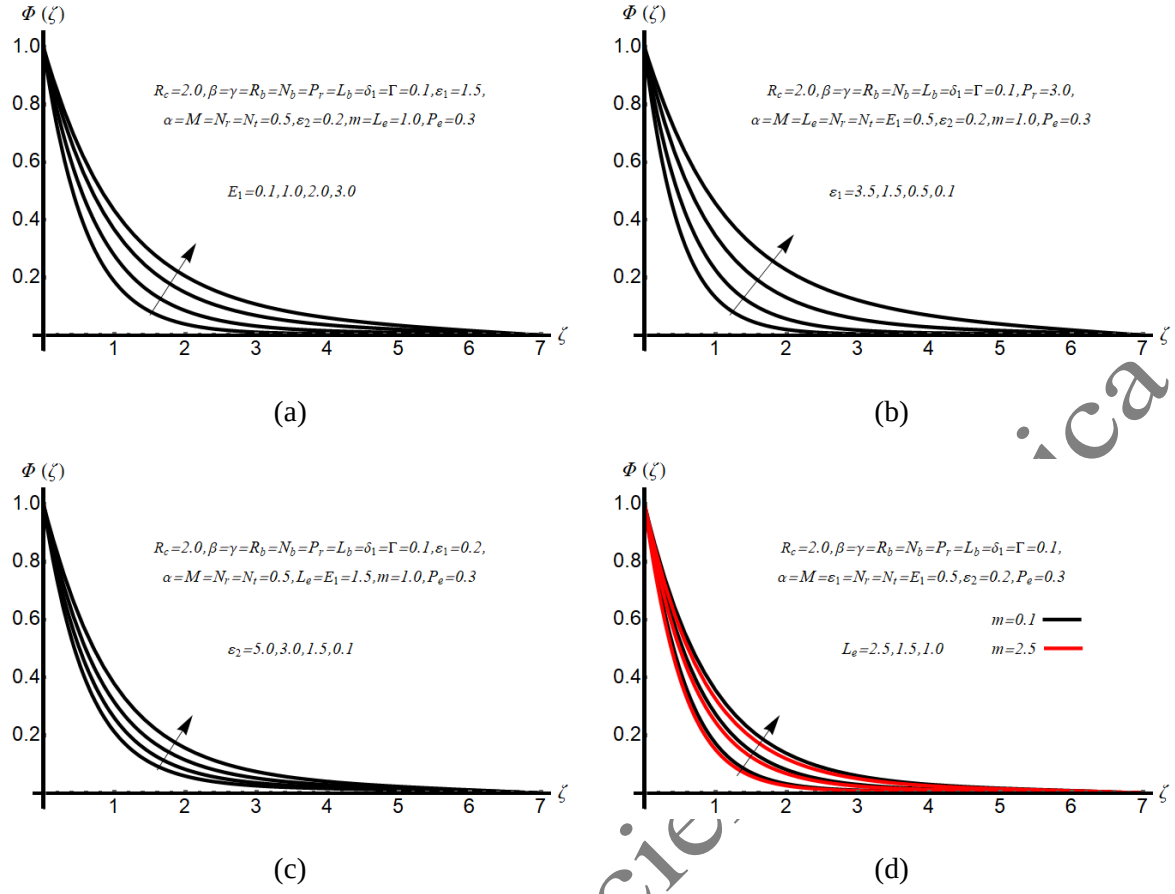
Φ (ζ)
1.0
0.8
0.6
0.4
0.2
1 2 3 4 5 6 7
ζ
$R_c=2.0,\beta=\gamma=R_b=N_b=P_r=L_b=\delta_1=\Gamma=0.1,\varepsilon_1=1.5,$
$\alpha=M=N_r=N_t=0.5,\varepsilon_2=0.2,m=L_e=1.0,P_e=0.3$
$E_1=0.1,1.0,2.0,3.0$
(a)
$R_c=2.0,\beta=\gamma=R_b=N_b=L_b=\delta_1=\Gamma=0.1,P_r=3.0,$
$\alpha=M=L_e=N_r=N_t=E_1=0.5,\varepsilon_2=0.2,m=1.0,P_e=0.3$
$\varepsilon_1=3.5,1.5,0.5,0.1$
(b)
$R_c=2.0,\beta=\gamma=R_b=N_b=P_r=L_b=\delta_1=\Gamma=0.1,\varepsilon_1=0.2,$
$\alpha=M=N_r=N_t=0.5,L_e=E_1=1.5,m=1.0,P_e=0.3$
$\varepsilon_2=5.0,3.0,1.5,0.1$
(c)
$R_c=2.0,\beta=\gamma=R_b=N_b=P_r=L_b=\delta_1=\Gamma=0.1,$
$\alpha=M=\varepsilon_1=N_r=N_t=E_1=0.5,\varepsilon_2=0.2,P_e=0.3$
$m=0.1$
$L_e=2.5,1.5,1.0$ $m=2.5$
(d)

Fig. 5

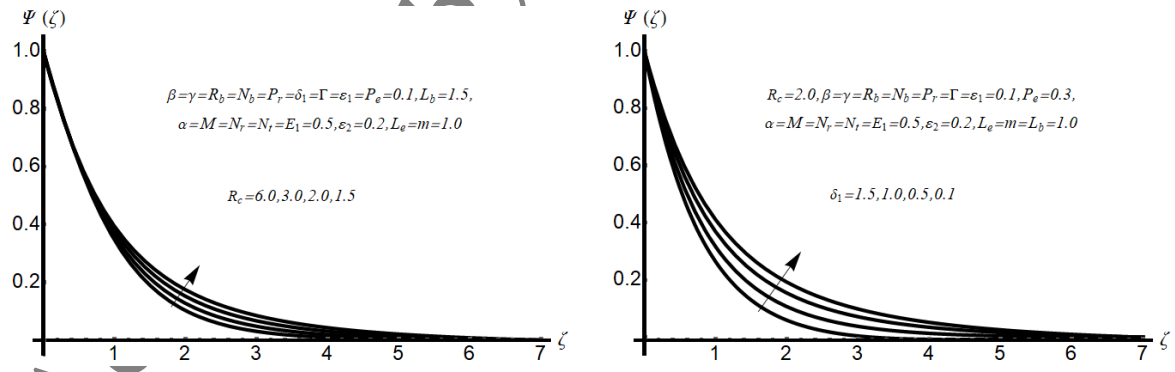
Ψ (ζ)
1.0
0.8
0.6
0.4
0.2
1 2 3 4 5 6 7
ζ
$\beta=\gamma=R_b=N_b=P_r=\delta_1=\Gamma=\varepsilon_1=P_e=0.1,L_b=1.5,$
$\alpha=M=N_r=N_t=E_1=0.5,\varepsilon_2=0.2,L_e=m=1.0$
$R_c=6.0,3.0,2.0,1.5$
(a)
$R_c=2.0,\beta=\gamma=R_b=N_b=P_r=\Gamma=\varepsilon_1=0.1,P_e=0.3,$
$\alpha=M=N_r=N_t=E_1=0.5,\varepsilon_2=0.2,L_e=m=L_b=1.0$
$\delta_1=1.5,1.0,0.5,0.1$
(b)

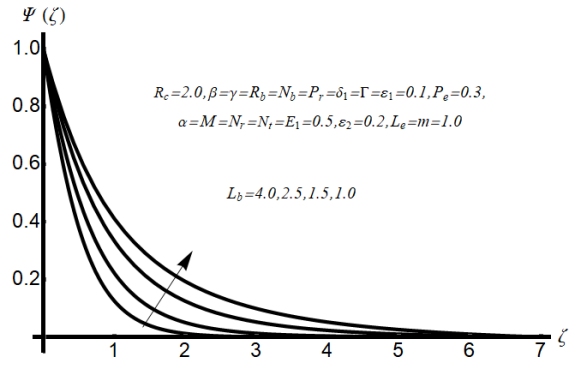

(c)

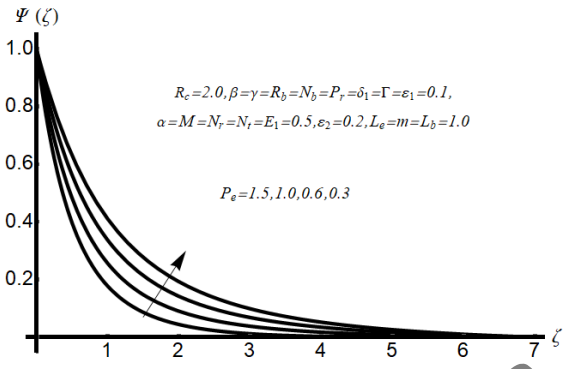

(d)

Fig. 6

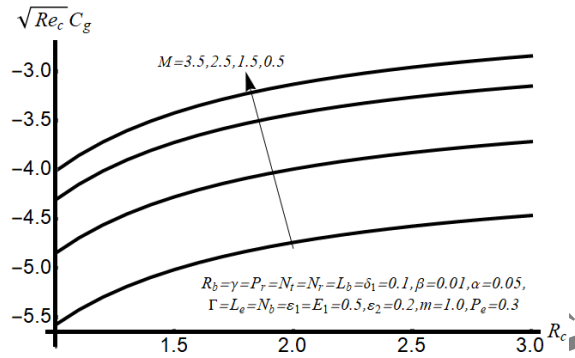

(a)

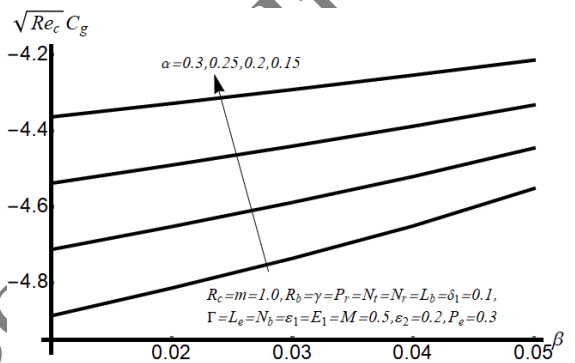

(b)

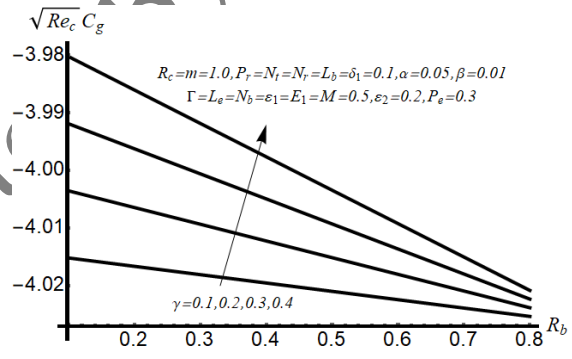

(c)

Fig. 7

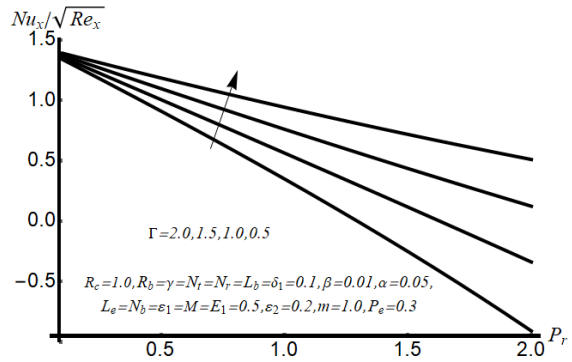

(a)

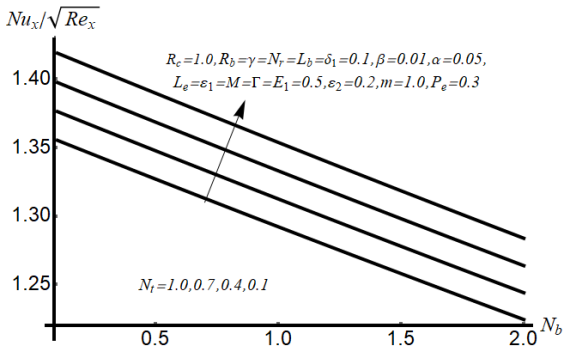

(b)

Fig. 8

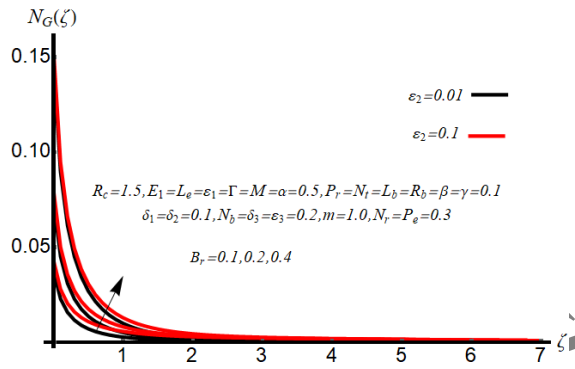

(a)

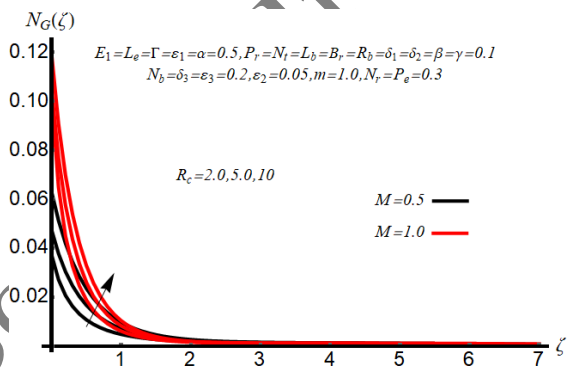

(b)

Fig. 9

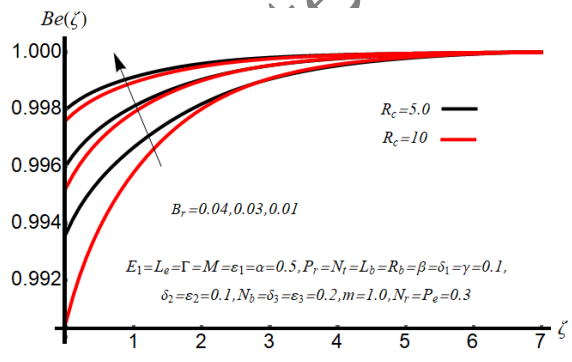

(a)

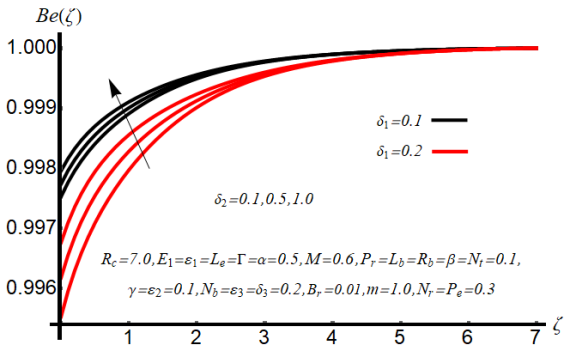

(b)

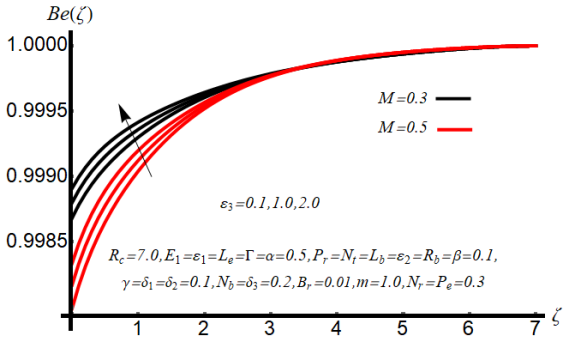

(c)

Fig. 10

Table 1: Comparison of numerical findings of $-\left(\sqrt{\mathrm{Re}_c}C_g\right)$ for divergent values of $\left(R_c\right)$ by keeping $M = N_r = \alpha = \beta = \gamma = R_b = P_r = L_b = P_e = \delta_1 = N_t = \Gamma = \varepsilon_1 = E_1 = N_b = m = \varepsilon_2 = 0$ fixed.

R_c		$-\left(\sqrt{\mathrm{Re}_c}C_g\right)$		
	Imran and Naveed [4]	Haq et al. [10]	Kumar et al. [15]	Present Results
5.0	1.15763	---	–1.157631	1.15763
10	1.07349	---	–1.073489	1.07349
20	1.03561	1.03562	–1.035609	1.03561
30	1.02353	1.02353	–1.023531	1.02353
40	1.01759	1.01759	–1.017587	1.01759
50	1.01405	1.01405	–1.014049	1.01405
100	1.00704	1.00704	–1.007038	1.00704
200	1.00356	1.00357	–1.003564	1.00356
1000	1.0008	---	–1.000799	1.0008

Table 2: Numerical findings for $S\,h_c / \sqrt{\mathrm{Re}_c}$ by keeping $M = N_r = 0.5, \alpha = 0.05, \beta = 0.01,$ $\gamma = R_b = \Gamma = P_r = L_b = \delta_1 = 0.1$, and P_e =0.3 fixed.

N_t	R_c	L_e	ε_1	N_b	m	ε_2	E_1	$Sh_c / \sqrt{\mathrm{Re}_c}$
0.1	2.0	0.5	0.1	0.2	1.0	0.2	0.1	1.30079
0.5								1.38833
0.9								1.57170
0.1	2.5							1.25695
	3.5							1.20567
	4.5							1.17659
	2.0	1.0						1.36188
		2.0						1.48396
		3.0						1.60562
		0.5	0.5					1.36896
			1.5					1.53206
			2.5					1.68577
			0.1	0.5				1.30052
				2.0				1.30028
				3.5				1.30014
				0.2	1.5			1.30201
					3.0			1.30622
					4.5			1.31146
					1.0	0.5		1.30434
						2.0		1.32206
						3.5		1.33971
						0.2	0.2	1.29935
							0.6	1.29468
							1.0	1.29138

Table 3: Numerical findings for $Mn_c / \sqrt{\mathrm{Re}_c}$ by keeping $M = N_r = 0.5, \alpha = 0.05, \beta = 0.01, \gamma = R_b = \Gamma = P_r = N_t = \Gamma = \varepsilon_1 = E_1 = 0.1, N_b = \varepsilon_2 = 0.2$, and m =1.0 fixed.

L_b	R_c	δ_1	P_e	$Mn_c / \sqrt{\mathrm{Re}_c}$
0.5	2.0	0.1	0.3	1.55173
2.0				1.69341
3.5				1.83775
0.5	2.5			1.49004
	3.5			1.41816
	4.5			1.37752
	2.0	0.2		1.56183
		0.6		1.60221
		1.0		1.64260
		0.1	0.1	1.36640
			0.4	1.64737
			0.7	1.94558